

Potential of sodium alginate/titanium oxide biomembrane nanocomposite in DMFC application

Norazuwana Shaari¹  | Siti Kartom Kamarudin^{1,2}  | Zulfirdaus Zakaria³ 

¹Fuel Cell Institute, Universiti Kebangsaan Malaysia, Bangi, Malaysia

²Department of Chemical and Process Engineering, Faculty of Engineering and Built Environment, Universiti Kebangsaan Malaysia, Bangi, Malaysia

³Institute of Sustainable Energy Kajang, Universiti Tenaga Nasional, Kajang, Malaysia

Correspondence

N. Shaari, Fuel Cell Institute, Universiti Kebangsaan Malaysia, 43600 UKM Bangi, Selangor, Malaysia.
Email: norazuwana.shaari@gmail.com

Funding information

Universiti Kebangsaan Malaysia (UKM), Grant/Award Numbers: MI-2018-006 and TRGS/1/2018/UKM/01/6/2

Summary

A proton exchange membrane was synthesized consuming a sodium alginate biopolymer as the matrix and titanium oxide as the nanofiller. The titanium oxide content varied from 5 to 25 wt%. The biomembrane nanocomposite performs better than the pristine sodium alginate membrane based on liquid uptake, methanol permeability, proton conductivity, ion exchange capacity, and oxidative stability outcomes. The unique properties of sodium alginate and titanium oxide lead to outstanding interconnections, thus producing new materials with great characteristics and enhanced performance. The highest proton conductivity achieved in this study is $17.3 \times 10^{-3} \text{ S cm}^{-1}$, which performed by SAT5 (25 wt%) membranes at 70°C. An optimal content of titanium oxide enhances the conductivity and methanol permeability of the membrane. Additionally, the hydrophilicity of pure sodium alginate is greatly reduced and achieves a good liquid uptake capacity and swelling ratio. The characteristics of the SA/TiO₂ biomembrane nanocomposite were determined with field emission scanning electron microscope, Fourier transform infrared, X-ray diffraction, thermal gravimetric analysis/differential scanning calorimetry, and mechanical strength analysis.

KEYWORDS

alginate, biomembrane, nanocomposite, titanium oxide

1 | INTRODUCTION

An electrochemical energy device of direct methanol fuel cells (DMFCs) is being researched, especially in the energy field, because of their convenient in-app availability in mobile devices, which appropriate with modern

lifestyles. In addition, high efficiency in the process of energy conversion as well as non-combustion processes have reduced greenhouse gas emissions causing DMFCs to be interested in addressing environmental issues.¹ In addition, the consumption of methanol as a fuel gives more advantage reduce the cost of fuel management

Nomenclature: DI, deionized; DMFC, direct methanol fuel cell; DSC, differential scanning calorimetry; Ea, activation energy; FESEM, field emission scanning electron microscope; FTIR, Fourier transform infrared; GO, graphene oxide; HPA, heteropolyacids; IEC, ion exchange capacity; L, distance between the two electrodes; OCV, open circuit voltage; P, membrane diffusion permeability for methanol; PBI, polybenzimidazole; PEMFC, polymer electrolyte membrane fuel cell; PEMs, proton exchange membrane; PSSA, poly-styrene sulfonic acid; PVA, poly vinyl alcohol; PVP, poly (vinylpyrrolidone); R, resistance of the membrane; RGO, reduced graphene oxide; SA, sodium alginate; SA/TiO₂, sodium alginate/titanium dioxide membrane; SGO, sulfonated graphene oxide; SPEEK, sulfonated poly (ether ether ketone); SPSF, sulfonated polysulfone; SW%, swelling ratio percentage; T, membrane thickness; TGA, thermal gravimetric analysis; T_g, glass transition temperature; TiO₂, titanium oxide; W, width of the membrane; WU%, water uptake percentage; XRD, X-ray diffraction

system which unrequired the external storage likes hydrogen, leads the flexibility of the cells designing, the fuel is exists in liquid phase and the refilling process of fuel is quick to supply the energy continuously.²⁻⁶ The membrane electrolyte assemble is the most important part of the DMFC and consists of electrodes (anodes and cathodes) that function as a centre for reactions and membranes that separate the anode and cathode; the membranes also serve as a barrier to the methanol trajectory as well as a pathway for protons, which are very important conductive agents.⁷⁻¹⁰ Nafion membranes are currently used because of their advantages over other membranes like excellent conductivity of proton, noble chemical, and physical stability.¹¹⁻¹³ Unfortunately, there are major disadvantages that prevent the continued commercialization of Nafion, which are expensive cost production and high crossover of methanol problems, which result in the loss of fuel and potential mixture on the cathode side, thereby reducing DMFC's overall performance. Besides, the oxidation process of methanol on the cathode side produced the excess water formation, which leads to the flooding phenomena on the cathode compartment. Thus, the cells are degraded and damaging the cathode area.¹⁴⁻¹⁷ It is therefore important for researchers to look for new membrane materials that have desirable properties, such as low permeability to methanol, low cost, high conductivity ($> 1.00 \times 10^{-3} \text{ S cm}^{-1}$), high thermal and mechanical resistance, and high chemical and physical stability.¹⁸⁻²⁰

Sodium alginate (SA) films are useful in many areas, including food packaging, medical applications, tissue engineering, separation, and fuel cells, due to their great potential to be made into various forms.²¹ Unfortunately, their application is still limited due to several weaknesses like being too hydrophilic and having undesirable mechanical properties.²² The most effective and useful method to produce enhanced polymer properties is blending or mixing two materials, as between polymers and nanoparticle fillers. The blended film usually has better mechanical properties and improved performance as well as physical appearance due to the combination and networking formed among the composites compared with those of a pure polymer.²³ Furthermore, the advantages of low cost and straightforward production of biopolymers make a blended membrane cost effective.²⁴ Several previous studies have been carried out on the combination of chitosan and SA biopolymers with nanofillers, which were carbon nanotube,²⁵ graphene,²⁶ titanium oxide,²⁷ zirconium,²⁸ and alumina.²⁹ There are several works that are explored the potential of SA biomembrane in DMFC application, Smitha et al³⁰ fabricated the poly-ion complex composite blend membrane with the chitosan. The blend

membrane showed the high conductivity of ion, low permeability of methanol, and high stability of mechanical. Mohanapriya et al³¹ blended the SA biomembrane with heteropolyacids (HPA) and synthetic polymer of poly (vinyl alcohol) (PVA). The mechanical strength and thermal stability of membrane have been enhanced attributed to the modification. Besides, the three-dimensional interaction of SA, PVA, and HPA is blocked the methanol tortuous across the composite membrane. Cabello et al³² explored the combination of two-type biopolymer, SA, and carrageenan. The introduction of carrageenan improved the conductivity of proton in range of $\sim 10^{-2} \text{ S cm}^{-1}$ and the permeability of methanol in range of $\sim 10^{-6} \text{ cm}^2 \text{ s}^{-1}$.

Since SA has disadvantages in terms of undesirable mechanical properties.³³ Titanium oxide (TiO_2) is an important ceramic material to enhance the polymer composite properties. The nanoparticle of TiO_2 has excellent chemical stability, high surface area, and activity, which influenced the properties of SA biopolymer chemically and physically. The modification of SA biopolymer with the hydrophilic TiO_2 will form a stable structure between the amorphous and crystalline regions required to upsurge the membrane conductivity and reduce the crossover of methanol. Besides, the addition of stiffer material of TiO_2 reduced effectively the swelling ratio of SA/ TiO_2 biomembrane nanocomposite. There are several bonding that leads in strong interaction among alginate polymer matrix and TiO_2 filler, for instance, dipole-dipole contact amid the attractive elements and van-der Waals force that inhibits the destroyed of polymer chain during the water absorption process. Rana et al³⁴ have explained about the interaction energy that build nonrandom spatial distribution among the polymer component according to the Flory-Huggins theory, which can be related to the interaction between TiO_2 nanofiller and SA polymer. Additionally, the immiscibility between SA polymer and TiO_2 also contribute in reduction of membrane swelling ratio with presence of TiO_2 .^{35,36}

Hence, the thermal stability, membrane dimension and cycle lifetime of SA/ TiO_2 can be improved significantly.³⁷⁻⁴⁰ This study aimed to fabricate the novel self-synthesis blended polymer membranes comprising natural SA polymers and titanium oxide nanofillers (designed as SA/ TiO_2 biomembrane nanocomposite). From the literature review, this is the first attempt that modified the SA biomembrane with the titanium oxide as a polymer electrolyte membrane in DMFC application. The new novel biomembrane nanocomposite properties are conducted, and their capability in DMFCs is determined through half-cell and single-cell electrolyte studies.

2 | MATERIALS

SA, titanium oxide (TiO₂), methanol (CH₃OH, 99.7%), glutaraldehyde (C₅H₈O₂), and glycerol (C₃H₈O₃) were attained from Sigma Aldrich. These chemicals were directly employed deprived of additional purification step.

3 | METHODOLOGY

SA (1.5 g) was diluted in deionized (DI) water (30 mL) with a constant stirring and uniform speed. Then, 10-mL mixture of DI water and titanium oxide solution was prepared and placed into the solution of SA with various weight percentages. The crosslinking and plasticizing agent consisting of a 1:1 volume ratio of glycerol and glutaraldehyde were poured into the solution. A sonicator was used to obtain a uniform solution of composite SA/titanium oxide. Then, the solution was poured into a petri dish for 48 hours at 60°C. The resultant composite film was taken out from the petri dish and refined using a procedure described in a previous paper.⁴¹

3.1 | Membrane characterization

The existence of functional groups in the SA/TiO₂ biomembrane was identified through Fourier transform infrared (FTIR) analysis (FTIR ELKER) with wavelengths 4000 to 500 cm⁻¹. A field emission scanning electron microscope (FEI QUANTA 400 field emission scanning electron microscope [FESEM]) was operated to identify the morphology and structure of the SA/TiO₂ biomembranes with 5 kV. A universal testing machine was used to measure the mechanical strength of the SA/TiO₂ biomembrane, specifically its tensile strength and elongation at break at ambient condition and with a 3-kN load.

The absorption of water rate can be calculated by the change in the weight of a wet vs dry membrane, while the swelling ratio property can be measured by the alteration in length (or thickness) membrane. Thus, the membrane was immersed in water for 48 hours at ambient condition. The access water was removed, and the weight and the length were recorded. Formerly, vacuum oven was employed for the membrane drying process at 100°C for 24-hour time. After drying, the length and weight of the membrane were also noted down. Calculation of water uptake (WU%) and swelling ratio (SW%) were carried out via Equations 1 and 2, where L_{wet} signifies the wet mass of membrane and L_{dry} signifies the dry condition gained as of the length of membranes in wet and dry condition, correspondingly:

$$\text{WU}\% = \frac{W_{\text{wet}} - W_{\text{dry}}}{W_{\text{dry}}} \times 100, \quad (1)$$

$$\text{SW}\% = \frac{L_{\text{wet}} - L_{\text{dry}}}{L_{\text{dry}}} \times 100. \quad (2)$$

A conductivity cell with four-electrode was used to calculate the membrane conductivity of proton and was linked to a potentiostat/galvanostat (WonATech) with a frequency range of 1 MHz down to 50 Hz. The conductivity of the protons was calculated in a wet membrane (size dimension = 1 cm × 4 cm), which 24-hour immersion in water afore tested. A graph of the voltage vs current was obtained from the potentiostat, and the slant of the straight line represented the membrane resistance. Using Equation 3, the proton conductivity can be measured:

$$\sigma = \frac{L}{RA}, \quad (3)$$

where L is the two electrodes distance, A is the area of membrane, and R is the membrane resistance.^{38,39} The membrane permeability of methanol was calculated by the difference in methanol concentration in two tanks that were marked as A and B . Equation 4 thus provides the permeability of methanol:

$$P = \frac{1}{Ca} \left(\frac{\Delta C_b(t)}{\Delta t} \right) \left(\frac{LVb}{A} \right), \quad (4)$$

where methanol permeability is signifies as P (cm²s⁻¹); Ca is the concentration of methanol in the feed chamber, ie, cell A (mol L⁻¹); $\Delta C_b(t)/\Delta t$ is the methanol molar concentration variation in cell B as a function of time (mol L⁻¹ s); V_b is the volume of each diffusion reservoir (cm³); A is the membrane area; and L is the membrane thickness (cm).

High conductivity of proton and low permeability of methanol lead to high selectivity of membrane, which is an indicator of good membrane characteristics. Equation 5 used for calculating the selectivity is as follows:

$$\alpha = \frac{\sigma}{P}, \quad (5)$$

where φ is represents selectivity, σ is represents proton conductivity, and P is represents methanol permeability.

4 | RESULT AND DISCUSSION

4.1 | FESEM

Figure 1 shows the surface with low magnification, cross section, and surface with high-magnification FESEM images of five membranes: Figures 1A to 1C for SAT1,

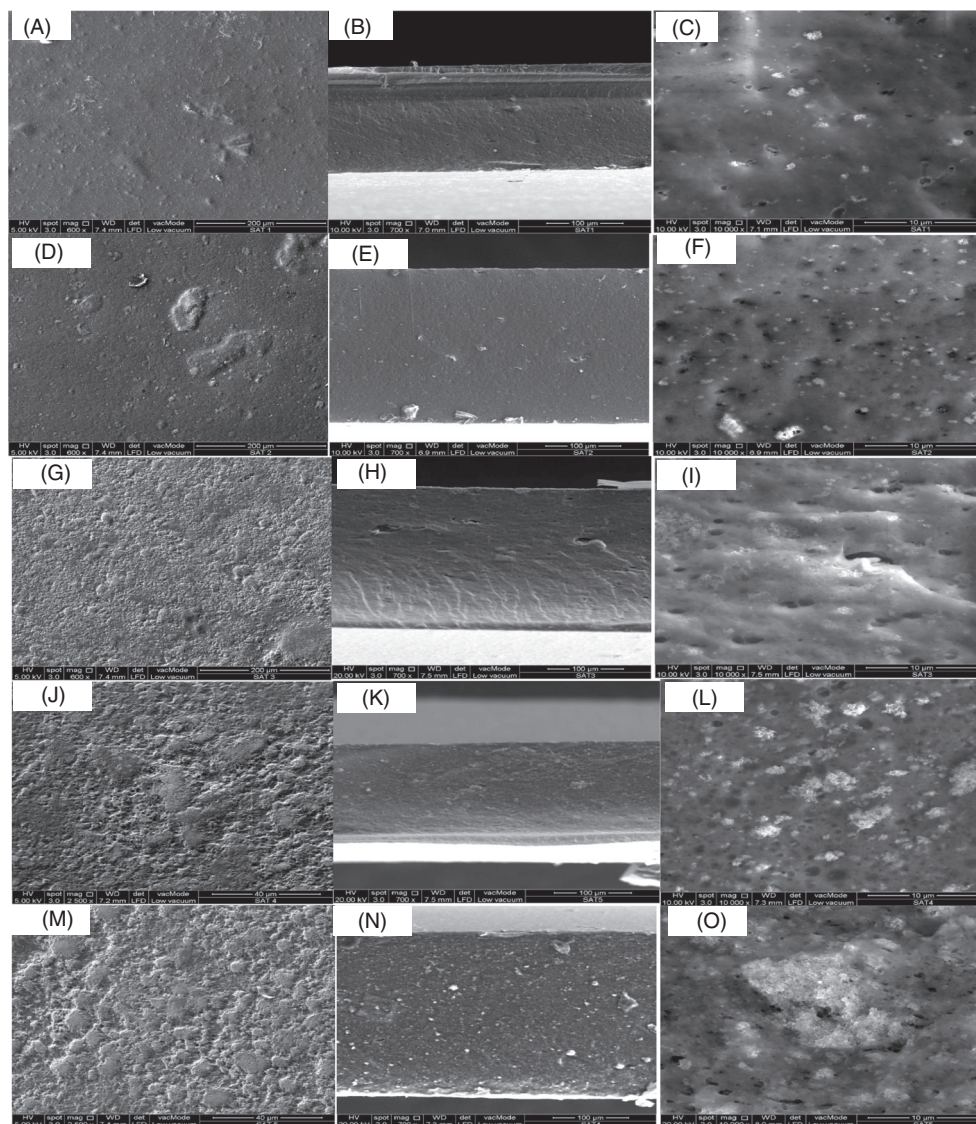


FIGURE 1 Field emission scanning electron microscope image of SA-TiO₂ membrane composite with various TiO₂ loading

Figures 1D to 1F for SAT2, Figures 1G to 1I for SAT3, Figures 1J to 1L for SAT4, and Figures 1M to 1O for SAT5, respectively. The uniform distribution of TiO₂ filler with optimum loading has resulting membrane the compress structures (nonporous) and a homogeneous morphology. The high homogeneity of membrane can be related to the high miscibility between SA polymer and TiO₂ nanofiller.³⁶ The solid membrane structure is a good feature for proton conductivity and reduces the rate of loss of methanol fuel. This polymer nanocomposite has a microstructure comprising interconnected SA biopolymer and TiO₂ inorganic nanofiller. The crystalline structure of TiO₂ changed the membrane morphology. The morphology of the SA membrane differs from other porous structure membranes, likes PBI and PIM-1 membranes,^{42,43} but it resembles a SPEEK membrane.⁴⁴ The homogeneous TiO₂ distribution increases the ion selectivity for the SA biomembrane. The membrane with the

loading of TiO₂ (20 wt%) has a higher TiO₂ nanoparticle density than the membrane with the lowest loading (5 wt%). However, the high TiO₂ loading (20 wt%) had a negative effect on the SA biomembrane structure because of agglomeration compared with other membranes that had a lower TiO₂ loading. The agglomeration also affected the properties of membrane, including proton conductivity and permeability, which are discussed in the next section. The SAT4 biomembrane shows the uniform structure, which formed the reliable structure, which has high potential to allow the proton diffusion pathway and provide the barrier for methanol crossover.

4.2 | X-ray diffraction

The structure of SA-TiO₂ membrane composite was determined with X-ray diffraction (XRD) analysis, as

shown in Figure 2. The XRD spectra are clearly visible from the peak at 2θ values of 19° and 25° and are from the TiO_2 nanoparticles,⁴⁵ while the peaks at 20° and 25° belong to the SA but have a very low intensity. The presence of TiO_2 increased the crystalline nature of the SA membrane compared with that of the pure SA membrane, which is similar to a previous study.⁴⁶ However, the TiO_2 crystalline peak has a low intensity compared with that of pure TiO_2 , possibly due to the low loading of TiO_2 and its homogeneous dispersion in the polymer matrix. The pure SA membrane XRD spectrum shows a low-intensity crystalline peak at 13.32° ; this is a naturally amorphous material with an intermolecular distance of 6.63 and thus is the same result that was reported in a previous study.⁵ However, the complete XRD spectrum shows that the SA/ TiO_2 membrane has amorphous structure properties,⁴⁷ indicating an interaction between the SA and TiO_2 nanoparticles.

4.3 | Thermal gravimetric analysis-differential scanning calorimetry

Thermal stability analysis results for SA-based membranes are presented in the TGA-DSC results, as shown in Figure 3. Below 200°C , the water passes through the evaporation process, leading to a small weight loss (1%), as revealed in the diagram. There is no detectable weight loss for this membrane composite at 150°C . SA usually experiences a heat decomposition process at 178°C , which is the first phase.⁴⁸ The SA TiO_2 membrane nanocomposite lost weight at higher temperatures for the first phase at 200°C , which shows the increasing the heat resistance of the membrane with the presence of TiO_2 nanofiller. Theoretically, weight loss at temperatures between 250 and 500°C is related to depolymerization and complex dehydration of the saccharide rings.⁴⁹ The

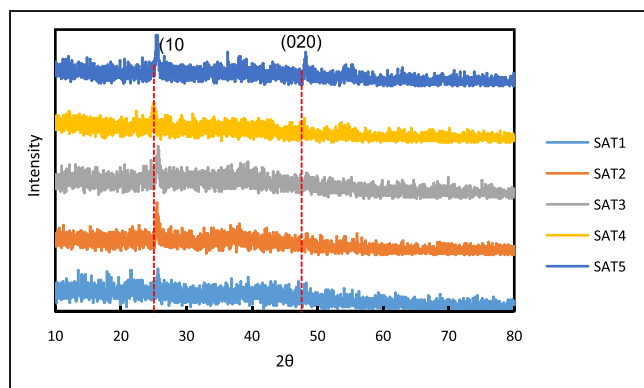


FIGURE 2 X-ray diffraction spectrum of SA- TiO_2 membrane composite with various TiO_2 loading [Colour figure can be viewed at wileyonlinelibrary.com]

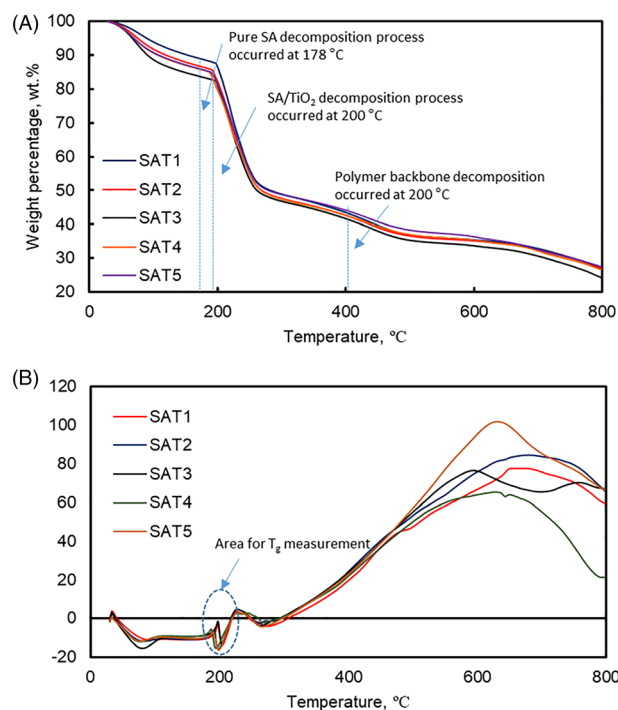


FIGURE 3 Thermal gravimetric analysis-differential scanning calorimetry spectrum of SA- TiO_2 membrane composite with various TiO_2 loading [Colour figure can be viewed at wileyonlinelibrary.com]

thermal stability of SA/ TiO_2 composite membrane became higher rather than pure SA, which attributed to the interfacial relations of electrostatic interaction and hydrogen-bonding interaction that occur between SA and TiO_2 ; these interactions are indispensable in DMFC applications operating at temperatures over 100°C . The decomposition of SA chain is possible, which causes weight loss in the second stage at 250°C temperature condition. Finally, the polymer backbone decomposition process that occurs causes the weight loss at a temperature of 400°C .⁵⁰ The T_g for SA, SAT1, SAT2, SAT3, SAT4, and SAT5 are 158 ,⁵¹ 206 , 203 , 200.67 , 198 , and 200.67°C , respectively. The interactions between TiO_2 and SA polymers reduced the internal rotation, which in turn affected the T_g value of the composite membrane. The T_g for a composite is needed for fuel cell applications to prevent thermal degradation of the membrane.⁵⁰

4.4 | FTIR

Figure 4 shows the FTIR spectrum for the SA membrane and SA/titanium oxide nanocomposite. The SA polymers have several common bands that were identified based on the functional groups present, like an OH stretching vibration, an asymmetric and symmetric COOA stretching vibration of the carboxylate salt group on the

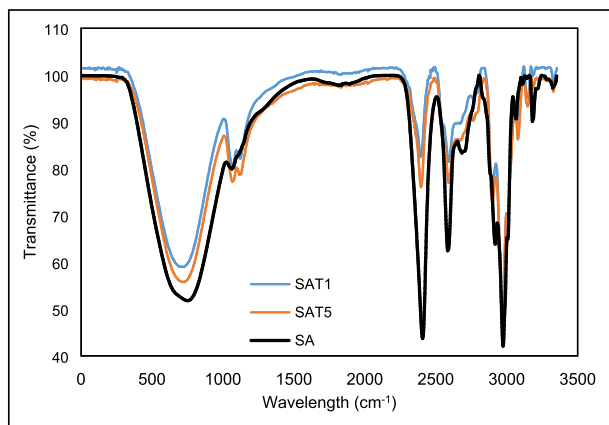


FIGURE 4 Fourier transform infrared spectrum of SA-TiO₂ membrane composite with various TiO₂ loading [Colour figure can be viewed at [wileyonlinelibrary.com](#)]

polymeric backbone, and a stretching vibration for COC groups at wavelengths of 3300, 1600, and 1410 cm⁻¹, 1030 cm⁻¹, respectively.⁵² For the polysaccharides, the peak is present at a wavelength of 1180-953 cm⁻¹ from the vibration of C-C, stretching of C-O, and the C-H bond bending mode. The presence of glycerol as a plasticizer in the membrane composite slightly changed the peak position of the wavelength compared with pure glycerol from 2936 and 2878 cm⁻¹ to 2986 and 2930 cm⁻¹, respectively. This change occurred due to the interaction of hydrogen bonding formation between SA and glycerol.⁵³ The presence of TiO₂ nanoparticles in the composite membrane also transformed the peak transmittance between 800 and 400 cm⁻¹, because it became a small, less intense, and wide curvature in the wavelength range of 400 to 600 cm⁻¹; the vibration of the Ti-O bonds was transverse thus leads in this curve shifting. Additionally, the longitudinal vibrational mode in 700 to 950 cm⁻¹ also led to a peak change in the SA/titanium oxide composite.⁴⁷

5 | MECHANICAL STRENGTH

The results of the mechanical strength of the fabricated membranes are represented in Figure 5. The increase of tensile strength property of SA biopolymer is increased with the TiO₂ loading in the membrane due to the relations formed amid the TiO₂ additive and the matrix. Wu et al⁵⁴ reported enhancement of membrane mechanical properties with the dispersion of TiO₂ in the polymer matrix, which acts as a physical cross-link to tolerate the external load. The hydrogen bonding formation is resulted in a robust interfacial linkage, which leads in superior mechanical properties. Besides, the synergy effect of TiO₂ filler and SA biopolymer matrix was a tad

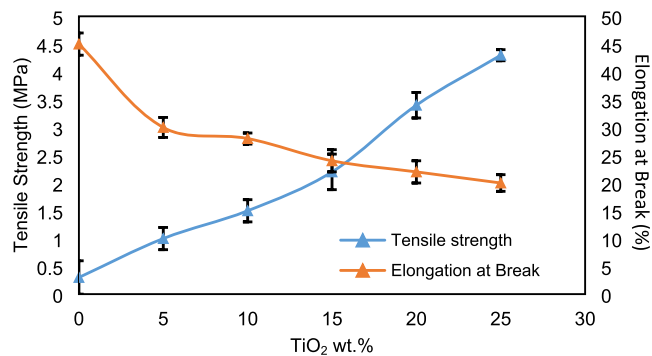


FIGURE 5 Tensile strength and elongation at break of SA-TiO₂ biomembrane composite with various TiO₂ loading [Colour figure can be viewed at [wileyonlinelibrary.com](#)]

increase the tensile strength of the biomembrane nanocomposite in the presence of TiO₂, which possess metallocene component. This component was positioned in free dimensions of SA biopolymer, which serve to obstacles the sliding of SA biopolymer molecule if any outer strength forced on membrane composite.⁵⁵⁻⁵⁷ In another study, Jafarzadeh et al⁵⁸ stated that the TiO₂ nanoparticle existence in polyethylene membrane has significantly increased the tensile strength. Table 1 listed the tensile stress for several biopolymer-based membrane such as chitosan, alginate, and carrageenan to compare the mechanical strength among them. The elongation at break of the SA-TiO₂ biomembrane composite is reduced due to the increase of inorganic particles, as presented in Figure 5. The huge feature fraction and interaction amid the polymer matrix and TiO₂ nanofiller are the big influencer on the elongation at break of SA biomembrane improved, consequently restrict the polymer chains alteration.^{61,62} Elongation at break is also known as flexibility. Logically, the higher the tensile strength or reinforcement effect is, the lower the flexibility the membrane. Thus, the results in this study are consistent with our understanding of polymer properties.

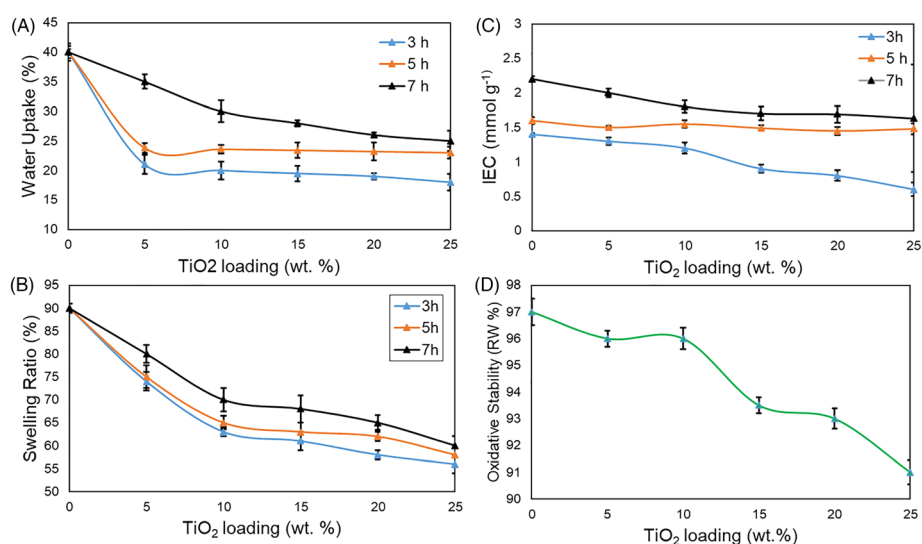
6 | WATER UPTAKE, SWELLING RATIO, IEC, AND OXIDATIVE STABILITY

Water is the most important component for life, and the proton exchange membrane also requires it to ensure that the proton is well conditioned based on the ability of the water to absorb the proton to be transferred.⁶³ A water uptake test with a SA-based membrane is presented in Figure 6A. In theory, it is evident that pure SA has a very high liquid uptake. The nanoparticle fillers present in the polymer matrix reduce the liquid uptake capacity.

TABLE 1 Comparison of proton conductivity and methanol permeability and selectivity of membranes based on biopolymeric membrane in DMFC

Membrane	Proton Conductivity, mS cm^{-1}	Methanol Permeability, $\times 10^{-6} \text{ cm}^2 \text{ s}^{-1}$	Selectivity, 10^4 S s cm^{-3}	Tensile Strength, MPa	Reference
SA/TiO ₂	16.8	0.195	8.615	4.3	Current study
SA/Glycerol	10.1	0.198	5.101	2.72	5
Pure SA	0.48	0.6	0.08	-	5
Alginate/Chitosan	42	4.1	1.023	72.29	30
Alginate/Carrageenan	31.6	4.89	0.646	28.03	32
SA/SGO	13.2	0.153	8.627	5.7	41
Chitosan/Zeolite	24	0.73	3.287	-	59
Nafion117	98.3	1.23	7.964	-	60

Abbreviation: DMFC: direct methanol fuel cell.

**FIGURE 6** Water uptake, swelling ratio, ion exchange capacity and oxidative stability of SA-TiO₂ membrane composite with various TiO₂ loading [Colour figure can be viewed at wileyonlinelibrary.com]

The TiO₂ filler functions as a blocker to molecules in the polymer matrix of SA, for example, water or methanol; instead, the membrane becomes warm or ionic or protonic.⁵ The higher the content of TiO₂ is, the lower the liquid absorption rate inside the membrane. The interaction between TiO₂ and SA is based on hydrogen bonding due to interfacial adhesion between the two components and results in a decreased liquid uptake capacity.⁶⁴ The OH⁻ groups in SA and -O- in TiO₂ are important groups for the formation of hydrogen bonds.^{4,64}

The presence of TiO₂ not only reduces liquid uptake but also increases the mechanical strength of the SA. The highest TiO₂ content shows the lowest swelling ratio result due to the blocking effect and a reduction in the membrane free volume, as presented in Figure 6B.³³ The present stiffer material of TiO₂ nanofiller is reduced effectively the swelling ratio of SA/TiO₂ biomembrane

nanocomposite. There are several formation bonding like the dipole-dipole interface reaction amid the van-der Waals force and attractive elements and that lead in strong interaction among SA biopolymer and TiO₂ nanofiller that inhibits the destroyed of polymer chain during the water absorption process. Rana et al³⁴ has explained about the interaction energy that build nonrandom spatial distribution among the polymer component according to the Flory-Huggins theory, which can be relate to TiO₂ nanofiller and SA polymer interaction. Additionally, the immiscibility between SA polymer and TiO₂ serves the reduction of the swelling ratio of membrane with presence of TiO₂.^{34-36,65}

Figure 6C represents the IEC value for the membranes, which were synthesized with different loading of TiO₂ nanofiller. The IEC increases with increasing TiO₂ until the loading decreases to 25 wt%. The quantity of

hydroxyl (OH⁻) in the SA/titanium oxide membrane is a major factor in the IEC value. As a result, the membrane conductivity of proton increases in parallel with the IEC value. By using the Fenton's reagent test method, the oxidative stability of the membranes is also considered in this study to determine the ability of the membranes to survive an attack by radical species, for instance (OH⁻ and OOH⁻), which is also referred to as the hastened oxidative stability test. Figure 6D shows the results from this oxidative stability test. Based on theory, radical species derive from the reactions that occur on the electrode. SAT5 membranes show the highest weight loss (9%) compared with that of the others after being immersed for 24 hours in Fenton's reagent. According to previous studies, when the IEC of the membrane is high, oxidative stability decreases. This trend is also true for this study. Nevertheless, the oxidative stability of the membranes in this study can still be categorized as good because less than 10% weight loss occurred, which is a good feature of proton exchange membranes. The membrane resistance towards the oxidation process of methanol reduces when the water uptake and swelling ratio increases. However, the oxidative stability is better than that of the pure SA biomembrane because the water uptake and swelling ratio improved. The weight loss may be due to a minor oxidative attack on the glutaraldehyde, calcium chloride, and glycerol crosslinkers. Additionally, the SA/TiO₂ biomembrane also presented the high chemical stability because it did not break and was still flexible even when soaked in 2 M methanol 60°C for 192 hours. This is a good achievement, especially for a biopolymer-based membrane.

7 | PROTON CONDUCTIVITY AND METHANOL PERMEABILITY

The error bars were included to present the performance test results such as water uptake, swelling ratio, methanol permeability, and proton conductivity. Error measurement shows that there is uncertainty during the calculation, which can be caused by several factors: (a) unequal membrane thickness, (ii) preparation of membrane also cannot avoid any errors such as dispersion filler or homogeneity, and (iii) pressure applied to the membrane when the membrane is mounted on the Teflon probe or in the chamber. All these factors affect the membrane performance test. However, this error can be ignored due to the very small error percentage between the repetition data.

The proton conductivity under various temperature conditions of SA/TiO₂ membrane is presented in Figure 7. The increases of temperature lead in the proton conductivity improvement, which is reliable with previous research by Shaari et al.⁴¹ and Zakaria et al.⁶⁶ Loading with 20 wt% TiO₂ achieved the highest proton conductivity at 30°C. The activation energy (E_a) of ionic transport for the SA/TiO₂ membrane can be calculated by applying the Arrhenius equation (Equation 6) to the Figure 7B, with the assumption that the conductivity obeys Arrhenius behaviour:

$$E_a = -b \times R \quad (6)$$

where b represents the slope of the regression line for $\ln \sigma$ (S/cm) vs $1000/T$ (K⁻¹) plots and R is the gas constant (8.314472 JK⁻¹ mol⁻¹).¹⁷ SAT1, SAT2, SAT3, SAT4, and

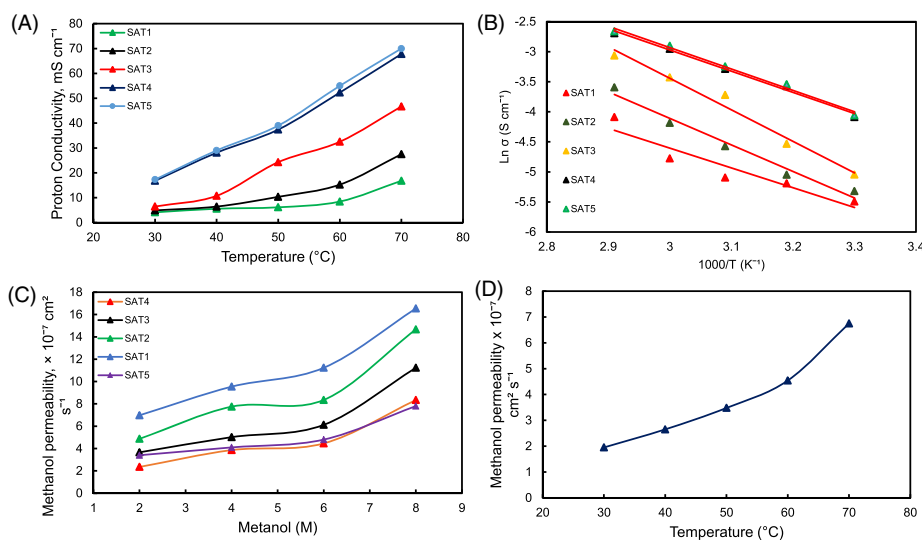
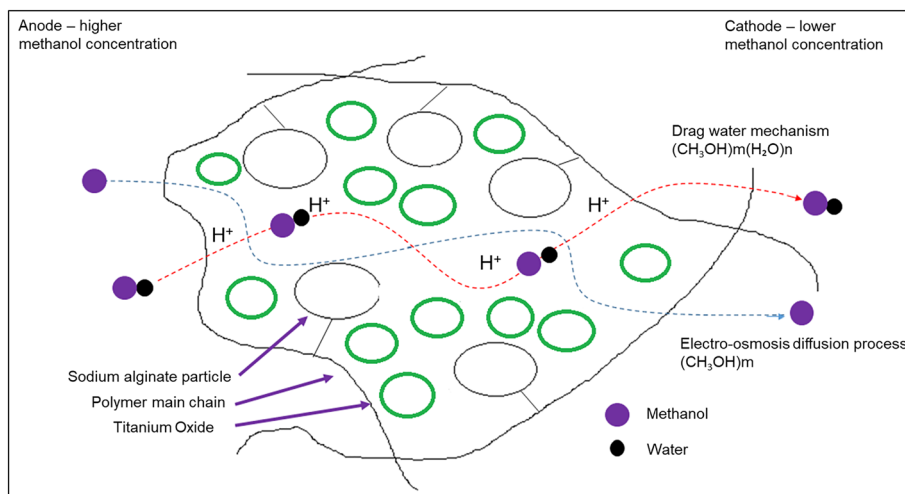


FIGURE 7 Proton conductivity and methanol permeability of SA/TiO₂ membrane composite with various TiO₂ loading [Colour figure can be viewed at wileyonlinelibrary.com]



SCHEME 1 Proton transfer mechanism [Colour figure can be viewed at wileyonlinelibrary.com]

SAT5 membrane exhibits an ion transport activation energy of 27.34, 36.73, 43.56, 29.54, and 29.34 J mol⁻¹ that is greater than Nafion 115 (6.00 kJ mol⁻¹)⁶⁷ and Nafion 117 (12 kJ mol⁻¹).⁶⁸

Hydrophilic SA coupled with titanium oxide holds water molecules, which ensures optimal hydrophilic based on their properties. Water-friendly properties are the main pillars to provide the pathways and movements of the protons in the membrane. Mechanisms for proton movement in SA/TiO₂ biomembrane nanocomposites are shown in Scheme 1. H⁺ has good interactions with O⁻ in TiO₂ through both mechanisms, namely, Grotthus and vehicle.

The SAT4 nanocomposite shows the lowermost methanol permeability (1.95×10^{-7} cm² s⁻¹) with a nanofiller loading amount of 20 wt% in 2 M methanol concentration as shown in Figure 7C. This low membrane permeability was due to the microstructure of the membrane that led to good networking between the SA and TiO₂ nanofiller; this is known as the blocking effect and was discussed in section above.⁶⁹ Different temperatures have different effects on the permeability of the membrane, as presented in Figure 7D. Increased temperatures led to increased methanol permeability for the membranes due to the structural changes in the biomembrane. Thermal energy provided at high temperatures increases the vibration of membrane chains and molecules, which was due to adding membrane free volume and reducing methanol rejection activity. It was easier to move methanol in the membrane due to a lack of internal resistance.⁷⁰ Gold nanoparticles inserted in the Nafion membrane functioned as methanol inhibitors, thus increasing overall performance, as reported in Mu et al.⁷¹

The formation of a hydrophilic passage in the SA membrane provides an easy way to move methanol; therefore, the titanium oxide nanofiller releases this space and reduces methanol permeability.^{64,72}

Table 1 lists the SAT4 membrane as the highest selectivity value of this study with the previous biomembrane based studies to make comparison. The selectivity value of SAT4 is equivalent with biomembrane previous studies, which shows the stable ratio in order to achieve the high proton conductivity and low the permeability of methanol. To evaluate the performance of this membrane, the passive DMFCs performance is tested. The

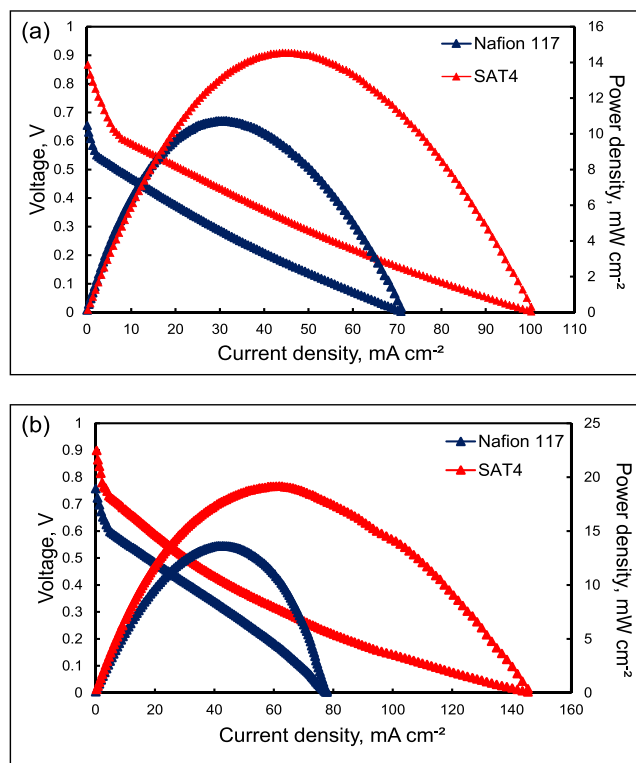


FIGURE 8 Cell voltage and power density vs. current density curve obtained for Nafion 117 and SAT4 membrane composite in 4M methanol concentration at temperature of (A) 30 and (B) 60°C [Colour figure can be viewed at wileyonlinelibrary.com]

TABLE 2 Comparison of condition in single-cell performance test with power density result for previous work and current study

Membrane	Anode Catalyst Loading, mg cm ⁻²	Cathode Catalyst Loading, mg cm ⁻²	Methanol Feed Concentration, mol dm ⁻³	Temperature, °C	P Max, mW cm ⁻²	Mode	Ref.
SA/glycerol	Pt-Ru:8	Pt:8	4	RT	2.99	Passive	⁵
SA/SGO	Pt-Ru:8	Pt:8	4	RT	13.6	Passive	⁴¹
SA/Carrageenan	Pt-Ru:5	Pt:5	2	50	10.4	Active	³²
Nafion 117	Pt-Ru:8	Pt:8	2	RT	7.95	Passive	⁷⁵
Nafion 117	Pt-Ru:8	Pt:8	2	RT	9.502	Passive	⁷⁷

selectivity value is the first expectation, which the high selectivity membrane will obtain the high power density of cells.^{59,60,73,74}

8 | SINGLE CELL

The SAT4 membrane single-cell performance in a passive mode was tested with the Nafion 117 membrane as the main indicator, and the result is plotted in Figures 8A and 8B. The conditions were 30°C and 4 M methanol for fuel concentration. Membrane SAT4 reaches the highest power density (14.53 mW cm⁻²) and current density (44.78 mAcm⁻²) with the best OCV (0.86 V) compared with those of the others, most likely influenced by the lowest methanol permeability performance. Nafion 117 obtains a lower OCV due to the high methanol permeability, because the methanol that crossed through the membrane theoretically decreases the OCV value. Nafion performed lower power density (10.73 mW cm⁻²) than SAT4 membrane; this is the good indicator of developed membrane potential. Thiam et al⁷⁵ and Chen et al⁷⁶ reported Nafion 117, and Nafion 115 reached 7.95 and 11 mW cm⁻² of the maximum power density, respectively. At higher temperature (60°C), the maximum power density of SAT4 and Nafion 117 reaches 19.13 and 13.63 mW cm⁻², respectively. Pure SA has a lower power density than Nafion or SAT4, indicating that the presence of TiO₂ particles helped in diffusion of proton transfer inside the matrix polymer as well as reducing permeability of methanol, consequently improving the whole DMFC performance. The small different of power density value amid the Nafion membrane and the membrane fabricated in this study shows that the SA/titanium dioxide membrane composite can be considered for future applications. However, these composite membrane modification efforts need to be continued to improve their performance. Table 2 lists several SA biopolymer-based membranes and their performance in a single-cell system.⁷⁷ It turns out that the membrane developed in this work is highly competitive compared with other membranes and is a viable alternative membrane for the future.

9 | CONCLUSION

The potential of SA based biomembrane especially in DMFC applications has been studied extensively in this study with the presence of titanium oxide nanofillers as additives and can be used as an important reference for the future research in fuel cell technology. Based on the author's knowledge, no such study was carried out before involving SA and titanium oxide as a biomembrane composite used in the DMFC application, which contained solid and broad discussions ranging from synthesis to single-cell performance testing. Both of these materials are categorized as cheap materials, which will overcome the high-cost problem for Nafion's commercial membrane. This is one of the great objectives of this study apart from improving the proton conductivity and reducing fuel crossover problems. The addition of TiO₂ inorganic nanofillers inside the alginate polymer matrices using convenient techniques yielded good results, such as an improvement in the ion exchange capacity property (the highest was 2.2 mmol g⁻¹), methanol permeability property (the lowest was 1.95 × 10⁻⁷ cm²s⁻¹), and proton conductivity property (the highest was 70 mScm⁻¹) compared with pure SA. Loading of 20 wt% TiO₂ also achieved over a 50% increase in the power density (19.13 mW cm⁻²) compared with that of the pure alginate membrane (2.99 mW cm⁻²). This performance of single cell test is considered outstanding in biomembrane category and yet higher than Nafion membrane (13.63 mW cm⁻²). These results show that the potential of SA biopolymer-based membrane is capable of becoming an alternative membrane, especially in DMFC systems, because it uses inexpensive and natural ingredients and is therefore a valuable discovery for future energy sources.

ACKNOWLEDGEMENT

The authors appreciatively recognize the monetary provision from Universiti Kebangsaan Malaysia (UKM) under MI-2018-006 and TRGS/1/2018/UKM/01/6/2.

ORCID

Norazuwana Shaari  <https://orcid.org/0000-0002-6900-9973>

Siti Kartom Kamarudin  <https://orcid.org/0000-0003-0383-5049>

Zulfirdaus Zakaria  <https://orcid.org/0000-0003-3292-8009>

REFERENCES

- Chen X, Li T, Shen J, Hu Z. From structures, packaging to application: a system-level review for micro direct methanol fuel cell. *Renew Sustain Energy Rev.* 2017;80:669-678.
- Ince AC, Karaoglan MU, Glösen A, Colpan CO, Müller M, Stolten D. Semiempirical thermodynamic modeling of a direct methanol fuel cell system. *Int J Energy Res.* 2019;43(8):3601-3615.
- Huo W, He H, Sun F. Microfluidic direct methanol fuel cell by electrophoretic deposition of platinum/carbon nanotubes on electrode surface. *Int J Energy Res.* 2015;39(10):1430-1436.
- Zakaria Z, Kamarudin SK, Timmiati S. Membranes for direct ethanol fuel cells: an overview. *Appl Energy.* 2016;163:334-342.
- Shaari N, Kamarudin SK, Basri S, Shyuan LK, Masdar MS, Nordin D. Enhanced mechanical flexibility and performance of sodium alginate polymer electrolyte bio-membrane for application in direct methanol fuel cell. *J Appl Polym Sci.* 2018;135(37):46666.
- Luo T, Xu H, Li Z, et al. Novel proton conducting membranes based on copolymers containing hydroxylated poly (ether ether ketone) and sulfonated polystyrenes. *J Appl Polym Sci.* 2017;134(34):45205.
- Scott K, Yu E, Vlachogiannopoulos G, Shivare M, Duteanu N. Performance of a direct methanol alkaline membrane fuel cell. *J Power Sources.* 2008;175(1):452-457.
- Headley AJ, Gross M, Chen D. Membrane electrolyte assembly health estimation method for proton exchange membrane fuel cells. *J Electrochem Energy Conv Storage.* 2017;14(4):041008.
- Shin H-S, Kwon O-J, Oh BS. Correlation between performance of polymer electrolyte membrane fuel cell and degradation of the carbon support in the membrane electrode assembly using image processing method. *Int J Hydrogen Energy.* 2018;43(45):20921-20930.
- Chen X, Shen J. Review of membranes in microfluidics. *J Chem Technol Biotechnol.* 2017;92(2):271-282.
- Janghorban K, Molla-Abbasi P. Modified CNTs/Nafion composite: the role of sulfonate groups on the performance of prepared proton exchange methanol fuel cell's membrane. *J Parenter Sci Technol.* 2018;3(4):211-218.
- Yan X, Wu R, Xu JB, Luo Z, Zhao TS. A monolayer graphene-Nafion sandwich membrane for direct methanol fuel cells. *J Power Sources.* 2016;311:188-194.
- Ru C, Gu Y, Duan Y, Zhao C, Na H. Enhancement in proton conductivity and methanol resistance of Nafion membrane induced by blending sulfonated poly (arylene ether ketones) for direct methanol fuel cells. *J Membr Sci.* 2019;573:439-447.
- Bukola S, Liang Y, Korzeniewski C, Harris J, Creager S. Selective proton/deuteron transport through Nafion/graphene/Nafion sandwich structures at high current density. *J Am Chem Soc.* 2018;140(5):1743-1752.
- Bae I, Oh KH, Yun SH, Kim H. Asymmetric silica composite polymer electrolyte membrane for water management of fuel cells. *J Membr Sci.* 2017;542:52-59.
- Wang Z, Zhang X, Nie L, Zhang Y, Liu X. Elimination of water flooding of cathode current collector of micro passive direct methanol fuel cell by superhydrophilic surface treatment. *Appl Energy.* 2014;126:107-112.
- Zhao T, Xu C, Chen R, Yang WW. Mass transport phenomena in direct methanol fuel cells. *Prog Energy Combust Sci.* 2009;35(3):275-292.
- Shaari N, Kamarudin SK. Chitosan and alginate types of bio-membrane in fuel cell application: an overview. *J Power Sources.* 2015;289:71-80.
- Ahmed M, Dincer I. A review on methanol crossover in direct methanol fuel cells: challenges and achievements. *Int J Energy Res.* 2011;35(14):1213-1228.
- Shaari N, Kamarudin SK. Recent advances in additive-enhanced polymer electrolyte membrane properties in fuel cell applications: An overview. *Int J Energy Res.* 2019;43(7):2756-2794.
- Shaari N, Kamarudin SK. Characterization studies of sodium alginate/sulfonated graphene oxide based polymer electrolyte membrane for direct methanol fuel cell. *Malaysian J Anal Sci.* 2017;21(1):113-118.
- Munavalli B, Torvi A, Kariduraganavar M. A facile route for the preparation of proton exchange membranes using sulfonated side chain graphite oxides and crosslinked sodium alginate for fuel cell. *Polymer.* 2018;142:293-309.
- Nagar H, Sumana C, Rao VB, Sridhar S. Performance evaluation of sodium alginate-Pebax polyion complex membranes for application in direct methanol fuel cells. *J Appl Polym Sci.* 2017;134(7):44485.
- Eldin MM, Hashem AE, Tamer TM, Omer AM, Yossuf ME, Sabet MM. Development of cross linked chitosan/alginate polyelectrolyte proton exchanger membranes for fuel cell applications. *Int J Electrochem Sci.* 2017;12:3840-3858.
- Karkeh-abadi F, Saber-Samandari S, Saber-Samandari S. The impact of functionalized CNT in the network of sodium alginate-based nanocomposite beads on the removal of Co (II) ions from aqueous solutions. *J Hazard Mater.* 2016;312:224-233.
- Zhuang Y, Yu F, Chen H, Zheng J, Ma J, Chen J. Alginate/graphene double-network nanocomposite hydrogel beads with low-swelling, enhanced mechanical properties, and enhanced adsorption capacity. *J Mater Chem A.* 2016;4(28):10885-10892.
- Idris A, Majidnia Z, Nor Kamarudin KSB. Photocatalyst treatment for lead (II) using titanium oxide nanoparticles embedded in PVA-alginate beads. *Desalin Water Treat.* 2016;57(11):5035-5044.
- Prabhu SM, Meenakshi S. Novel one-pot synthesis of dicarboxylic acids mediated alginate-zirconium biopolymeric complex for defluoridation of water. *Carbohydr Polym.* 2015;120:60-68.
- Gopalakannan V, Periyasamy S, Viswanathan N. One pot eco-friendly synthesis of highly dispersed alumina supported alginate biocomposite for efficient chromium (VI) removal. *J Water Process Eng.* 2016;10:113-119.

30. Smitha B, Sridhar S, Khan A. Chitosan–sodium alginate polyion complexes as fuel cell membranes. *Eur Polym J*. 2005;41(8):1859-1866.
31. Mohanapriya S, Bhat SD, Sahu AK, et al. Sodium-alginate-based proton-exchange membranes as electrolytes for DMFCs. *Energ Environ Sci*. 2010;3(11):1746-1756.
32. Cabello SP, Mollá S, Ochoa NA, Marchese J, Giménez E, Compañ V. New bio-polymeric membranes composed of alginate-carrageenan to be applied as polymer electrolyte membranes for DMFC. *J Power Sources*. 2014;265:345-355.
33. Ionita M, Pandele MA, Iovu H. Sodium alginate/graphene oxide composite films with enhanced thermal and mechanical properties. *Carbohydr Polym*. 2013;94(1):339-344.
34. Rana D, Mandal B, Bhattacharyya S. Analogue calorimetric studies of blends of poly (vinyl ester) s and polyacrylates. *Macromolecules*. 1996;29(5):1579-1583.
35. Rana D, Mandal B, Bhattacharyya S. Miscibility and phase diagrams of poly (phenyl acrylate) and poly (styrene-co-acrylonitrile) blends. *Polymer*. 1993;34(7):1454-1459.
36. Rana D, Bag K, Bhattacharyya SN, Mandal BM. Miscibility of poly (styrene-co-butyl acrylate) with poly (ethyl methacrylate): Existence of both UCST and LCST. *J Polym Sci B*. 2000;38(3):369-375.
37. Yang C-C, Chiu SJ, Lee KT, Chien WC, Lin CT, Huang CA. Study of poly (vinyl alcohol)/titanium oxide composite polymer membranes and their application on alkaline direct alcohol fuel cell. *J Power Sources*. 2008;184(1):44-51.
38. Cozzi D, de Bonis C, D'Epifanio A, Mecheri B, Tavares AC, Licoccia S. Organically functionalized titanium oxide/Nafion composite proton exchange membranes for fuel cells applications. *J Power Sources*. 2014;248:1127-1132.
39. Pinar FJ, Cañizares P, Rodrigo MA, Ubada D, Lobato J. Titanium composite PBI-based membranes for high temperature polymer electrolyte membrane fuel cells. Effect on titanium dioxide amount. *RSC Adv*. 2012;2(4):1547-1556.
40. Lobato J, Cañizares P, Rodrigo MA, Úbeda D, Pinar FJ. A novel titanium PBI-based composite membrane for high temperature PEMFCs. *J Membr Sci*. 2011;369(1-2):105-111.
41. Shaari N, Kamarudin SK, Basri S, Shyuan LK, Masdar MS, Nordin D. Enhanced proton conductivity and methanol permeability reduction via sodium alginate electrolyte-sulfonated graphene oxide bio-membrane. *Nanoscale Res Lett*. 2018;13(1):82.
42. Chae IS, Luo T, Moon GH, Ogieglo W, Kang YS, Wessling M. Ultra-high proton/vanadium selectivity for hydrophobic polymer membranes with intrinsic nanopores for redox flow battery. *Adv Energy Mater*. 2016;6(16):1600517.
43. Luo T, David O, Gendel Y, Wessling M. Porous poly (benzimidazole) membrane for all vanadium redox flow battery. *J Power Sources*. 2016;312:45-54.
44. Ji Y, Tay ZY, Li SFY. Highly selective sulfonated poly (ether ether ketone)/titanium oxide composite membranes for vanadium redox flow batteries. *J Membr Sci*. 2017;539:197-205.
45. Park N-G, Schlichthörl G, van de Lagemaat J, Cheong HM, Mascarenhas A, Frank AJ. Dye-sensitized TiO₂ solar cells: structural and photoelectrochemical characterization of nanocrystalline electrodes formed from the hydrolysis of TiCl₄. *J Phys Chem B*. 1999;103(17):3308-3314.
46. Lokesh B, Rao KK, Reddy KM, Rao KC, Rao PS. Novel nanocomposite membranes of sodium alginate filled with polyaniline-coated titanium dioxide for dehydration of 1, 4-dioxane/water mixtures. *Desalination*. 2008;233(1-3):166-172.
47. Di Vona M, Sgreccia E, Donnadio A, et al. Composite polymer electrolytes of sulfonated poly-ether-ether-ketone (SPEEK) with organically functionalized TiO₂. *J Membr Sci*. 2011;369(1-2):536-544.
48. Paşcalău V, Popescu V, Popescu GL, et al. The alginate/k-carrageenan ratio's influence on the properties of the cross-linked composite films. *J Alloys Compd*. 2012;536:S418-S423.
49. Haldorai Y, Shim JJ. Novel chitosan-TiO₂ nanohybrid: preparation, characterization, antibacterial, and photocatalytic properties. *Polym Compos*. 2014;35(2):327-333.
50. Zhang J, Lan F, Liang D, Xiao Y, Lu S, Xiang Y. Bulk modification of Nafion® with purple membrane for direct methanol fuel cell applications. *J Membr Sci*. 2011;382(1-2):350-354.
51. Roger S, Bee A, Balnois E, Bourmaud A, Le Deit H, Grohens Y. Physical and mechanical properties of alginate films containing calcium cations and ferrofluids. In 5th International Conference on Polymer-Solvent Complexes & Intercalates. 2003.
52. Nie L, Liu C, Wang J, Shuai Y, Cui X, Liu L. Effects of surface functionalized graphene oxide on the behavior of sodium alginate. *Carbohydr Polym*. 2015;117:616-623.
53. Talja RA, Helén H, Roos YH, Jouppila K. Effect of various polyols and polyol contents on physical and mechanical properties of potato starch-based films. *Carbohydr Polym*. 2007;67(3):288-295.
54. Wu G, Gan S, Cui L, Xu Y. Preparation and characterization of PES/TiO₂ composite membranes. *Appl Surf Sci*. 2008;254(21):7080-7086.
55. Rana D, Sauvant V, Halary J. Molecular analysis of yielding in pure and antiplasticized epoxy-amine thermosets. *J Mater Sci*. 2002;37(24):5267-5274.
56. Rana D, Kim HL, Kwag H, Choe S. Hybrid blends of similar ethylene 1-octene copolymers. *Polymer*. 2000;41(19):7067-7082.
57. Rana D, Kim HL, Kwag H, et al. Blends of ethylene 1-octene copolymer synthesized by Ziegler–Natta and metallocene catalysts. II. Rheology and morphological behaviors. *J Appl Polym Sci*. 2000;76(13):1950-1964.
58. Jafarzadeh Y, Yegani R, Tantekin-Ersolmaz S. Effect of TiO₂ nanoparticles on structure and properties of high density polyethylene membranes prepared by thermally induced phase separation method. *Polym Adv Technol*. 2015;26(4):392-398.
59. Wang J, Zheng X, Wu H, et al. Effect of zeolites on chitosan/zeolite hybrid membranes for direct methanol fuel cell. *J Power Sources*. 2008;178(1):9-19.
60. Cao K, Jiang Z, Zhao J, et al. Enhanced water permeation through sodium alginate membranes by incorporating graphene oxides. *J Membr Sci*. 2014;469:272-283.
61. Rana D, Cho K, Woo T, Lee BH, Choe S. Blends of ethylene 1-octene copolymer synthesized by Ziegler–Natta and metallocene catalysts. I. Thermal and mechanical properties. *J Appl Polym Sci*. 1999;74(5):1169-1177.

62. Rana D, Lee CH, Cho K, Lee BH, Choe S. Thermal and mechanical properties for binary blends of metallocene polyethylene with conventional polyolefins. *J Appl Polym Sci*. 1998;69(12):2441-2450.
63. You P, Kamarudin S, Masdar M. Improved performance of sulfonated polyimide composite membranes with rice husk ash as a bio-filler for application in direct methanol fuel cells. *Int J Hydrogen Energy*. 2019;44(3):1857-1866.
64. Shirdast A, Sharif A, Abdollahi M. Effect of the incorporation of sulfonated chitosan/sulfonated graphene oxide on the proton conductivity of chitosan membranes. *J Power Sources*. 2016;306:541-551.
65. Rana D, Mandal B, Bhattacharyya S. Analogue calorimetry of polymer blends: poly (styrene-co-acrylonitrile) and poly (phenyl acrylate) or poly (vinyl benzoate). *Polymer*. 1996;37(12):2439-2443.
66. Zakaria Z, Kamarudin S, Timmiati S. Influence of graphene oxide on the ethanol permeability and ionic conductivity of QPVA-based membrane in passive alkaline direct ethanol fuel cells. *Nanoscale Res Lett*. 2019;14(1):28.
67. Slade RC, Varcoe JR. Investigations of conductivity in FEP-based radiation-grafted alkaline anion-exchange membranes. *Solid State Ion*. 2005;176(5-6):585-597.
68. Li YS, Zhao TS. A passive anion-exchange membrane direct ethanol fuel cell stack and its applications. *Int J Hydrogen Energy*. 2016;41(44):20336-20342.
69. Heo Y, Im H, Kim J. The effect of sulfonated graphene oxide on sulfonated poly (ether ether ketone) membrane for direct methanol fuel cells. *J Membr Sci*. 2013;425:11-22.
70. Xiong Y, Fang J, Zeng QH, Liu QL. Preparation and characterization of cross-linked quaternized poly (vinyl alcohol) membranes for anion exchange membrane fuel cells. *J Membr Sci*. 2008;311(1-2):319-325.
71. Mu S, Tang H, Wan Z, Pan M, Yuan R. Au nanoparticles self-assembled onto Nafion membranes for use as methanol-blocking barriers. *Electrochem Commun*. 2005;7(11):1143-1147.
72. Pawar SN, Edgar KJ. Alginate derivatization: a review of chemistry, properties and applications. *Biomaterials*. 2012;33(11):3279-3305.
73. Zakaria Z, Kamarudin SK. Performance of quaternized poly (vinyl alcohol)-based electrolyte membrane in passive alkaline DEFCs application: RSM optimization approach. *J Appl Polym Sci*. 2019;136(19):47526.
74. Zakaria Z, Shaari N, Kamarudin SK. Preliminary study of alkaline direct ethanol fuel cell by using crosslinked quaternized poly (vinyl alcohol)/graphene oxide membrane. *J Kejuruteraan*. 2018;30(2):219-227.
75. Thiam H, Daud WR, Kamarudin SK, et al. Nafion/Pd-SiO₂ nanofiber composite membranes for direct methanol fuel cell applications. *Int J Hydrogen Energy*. 2013;38(22):9474-9483.
76. Chen W, Yuan W, Ye G, Han F, Tang Y. Utilization and positive effects of produced CO₂ on the performance of a passive direct methanol fuel cell with a composite anode structure. *Int J Hydrogen Energy*. 2017;42(23):15613-15622.
77. Shaari N, Kamarudin SK. Performance of crosslinked sodium alginate/sulfonated graphene oxide as polymer electrolyte membrane in DMFC application: RSM optimization approach. *Int J Hydrogen Energy*. 2018;43(51):22986-23003.

How to cite this article: Shaari N, Kamarudin SK, Zakaria Z. Potential of sodium alginate/titanium oxide biomembrane nanocomposite in DMFC application. *Int J Energy Res*. 2019;43:8057-8069. <https://doi.org/10.1002/er.4801>